doi:10.1016/j.jmb.2009.11.016 J. Mol. Biol. (2010) 395, 916–923

JMB

Available online at www.sciencedirect.com

ScienceDirect

ELSEVIER

COMMUNICATION

Dynamic Allostery Controls Coat Protein Conformer Switching during MS2 Phage Assembly

E. C. Dykeman[1], P. G. Stockley[2] and R. Twarock[1]*

[1]*York Centre for Complex Systems Analysis, University of York, York YO10 5DD, UK*

[2]*Astbury Centre for Structural Molecular Biology, University of Leeds, Leeds LS2 9JT, UK*

Received 17 August 2009; received in revised form 2 November 2009; accepted 5 November 2009
Available online 12 November 2009

Previously, an RNA stem–loop (TR) encompassing 19 nt of the genome of bacteriophage MS2 was shown to act as an allosteric effector of conformational switching in the coat protein during *in vitro* capsid assembly. TR RNA binding to symmetric coat protein dimers results in conformational changes, principally at the FG-loop connecting the F and G β-strands in each subunit, yielding an asymmetric structure. The FG-loops define the quasi-equivalent conformers of the coat protein subunit (A, B, and C) in the $T=3$ capsid. Efficient assembly of this capsid *in vitro* requires that both symmetrical and asymmetrical forms of the coat protein dimer be present in solution, implying that they closely resemble the quasi-equivalent dimers (A/B and C/C) seen in the final capsid. Experiments show that assembly can be triggered by a number of RNA stem–loops unrelated to TR in sequence and detailed secondary structure, suggesting that there is little sequence specificity to the allosteric effect. Since the stem–loop binding site on the coat protein dimer is distal to the FG-loops the mechanism of this switching effect needs to be investigated. We have analyzed the vibrational modes of both TR-bound and RNA-free coat protein dimers using an all-atom normal-mode analysis. The results suggest that asymmetric contacts between the A-duplex RNA phosphodiester backbone and the EF-loop in one coat protein subunit result in the FG-loop of that subunit becoming more dynamic, whilst the equivalent loop on the other monomer decreases its mobility. The increased dynamic behaviour occurs in the FG-loop of the subunit required to undergo the largest conformational change when adopting the quasi-equivalent B conformation. The free energy barrier on the pathway to form this new structure would consequently be reduced compared to the unbound subunit. Our results also imply that the allosteric effect should be independent of the base sequence of the bound stem–loop, as observed experimentally. As a test of this model, we also examined the vibrational modes of a known assembly mutant, W82R, which cannot assemble beyond dimer. This mutation leads to an increased mobility of the DE-loop rather than the FG-loop after TR binding, consistent with the non-assembling phenotype of this mutant protein.

Keywords: dynamic allostery; virus assembly; RNA–protein interaction; RNA bacteriophage; conformational change

Edited by D. E. Draper

Bacteriophage[1,2] MS2 is a model for the study of single-stranded RNA virus assembly as it provides important insights on the multiple roles of viral RNA in the assembly process.[3,4] It comprises a $T=3$ particle formed from three quasi-equivalent conformers (A, B, and C) that are organized in 60 asymmetric A/B dimers surrounding its 5-fold symmetry axes, and 30 symmetric C/C dimers located on its 2-fold axes (see Fig. 1). The main structural differences between these dimers are in the conformations of their FG-loops, connecting the F and G β-strands of each subunit: in the B subunit the FG-loop is in a folded conformation, whilst the FG-loops of the A and C conformers are extended (Fig. 1a and b). Assembly of the $T=3$ capsid requires the correct placement of both symmetric and

*Corresponding author. E-mail address: rt507@york.ac.uk.

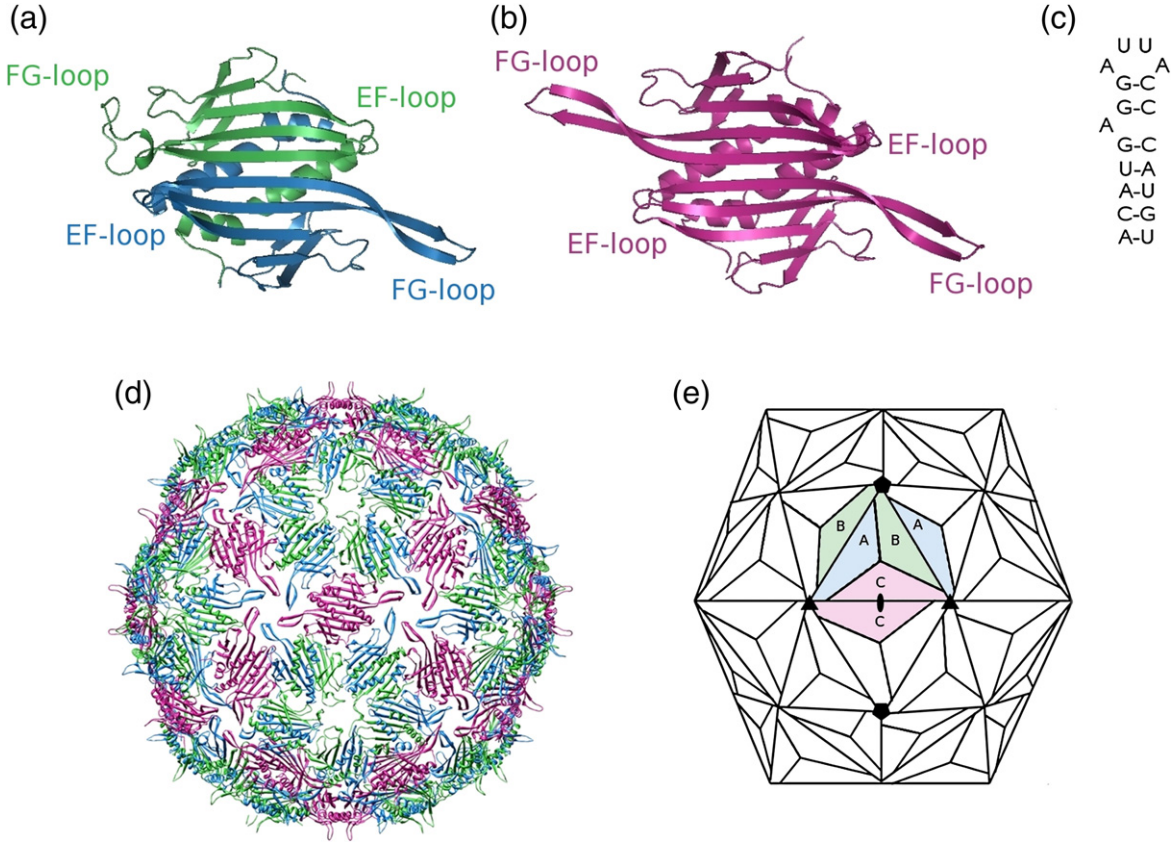

Fig. 1. Structures of MS2 coat protein dimers, TR, and $T=3$ capsid. The three quasi-equivalent protein conformers, chains A, B, and C, are shown in blue, green, and magenta, respectively. (a) Ribbon diagram of an A/B dimer from the capsid with one folded and one extended FG-loop. (b) As in (a) for the C/C dimer with two extended FG-loops. (c) Sequence and secondary structure of the TR RNA fragment. (d) Crystal structure of the MS2 capsid (1ZDH) showing the positions of the A/B and C/C dimers. (e) Diagram illustrating the placements of these dimers with respect to the icosahedral shell. The B subunits of five A/B dimers meet at the 5-fold symmetry axes, whilst one C/C dimer is placed at each 2-fold symmetry axis.

asymmetric dimers. Efficient assembly can be promoted by triggering the conversion of a proportion of symmetric C/C dimers, the predominant conformation found in solution, into asymmetric A/B dimers.[5] A high-affinity 19-nt RNA stem–loop (TR) in the genome of the phage was shown previously to cause such a conformational change. Basnak *et al.*[6] demonstrate that multiple other stem–loops, unrelated in detail to TR, can trigger the same effect, suggesting that it is not sequence-specific. Since the FG-loops are >12 Å away from the binding site of the RNA on the dimer, the conformational switch appears to be due to an allosteric effect. The molecular basis of this switch and the reasons for its apparent lack of sequence specificity are currently unknown. We address both questions below using an all-atom normal-mode analysis with an empirical force field.

A mutant coat protein, W82R, has been characterized that does not assemble beyond dimer despite the fact that it binds TR.[6,7] This shows that the allosteric effect is sensitive to the nature of the amino acid side chains in the coat protein, requiring any theoretical analysis to include all protein atoms. Due to the computational complexity of handling large viral protein structures, previous attempts in normal-mode analysis have centered around the use of different degrees of coarse-graining, for example, by considering only C_α atoms.[8] We attempted to study the allosteric effect here using an elastic network model, but this proved unsuccessful. We therefore employed a novel technique that we (E.C.D.) recently designed to perform a fully atomistic analysis of the lowest-frequency normal modes based on the AMBER empirical energy model.[9] It provides quantitative estimates of the frequencies associated with normal modes that are critical for predicting the amplitudes of each mode and the average fluctuations of atoms in the structure about equilibrium.

An all-atom normal-mode analysis of a C/C dimer in complex with a TR stem loop (bound state) was performed and compared with the corresponding analysis of the C/C dimer alone (unbound state). The all-atom normal-mode analysis requires a minimized structure to determine reliable frequencies. Using the AMBER force field[10] with the generalized Born implicit solvent model,[11] we minimized the 2.7 Å resolution X-ray structure (1ZDH)[12] of the C/C dimer with and without bound TR to an RMS force less than 10^{-6} kcal mol^{-1} Å^{-1}. The starting model for the TR-bound C/C dimer was based on the X-ray structure of recombinant

capsids soaked with RNA fragments encompassing the TR sequence. In these particles, TR binds in both orientations underneath C/C dimers but the density is not overlapped in the upper stem and loop regions, allowing unambiguous modeling of this complex.[12] Hydrogen atoms were added following the known structures of the residues at pH 7 before performing the minimization and normal-mode analysis procedures. The resulting all-atom RMSD between the X-ray and the minimized structures was less than 1.53 Å. The shift of the atomic positions from the X-ray coordinates is hence small when compared to the resolution of 2.7 Å, and is consistent with the RMSD of minimized structures from other normal-mode analyses done on viruses.[13] Using the lowest 100 eigenvalues $e_v(i)$ and frequencies ω_v, we computed the dynamic fluctuation around equilibrium of each atom i, located at position r_i, according to:

$$\langle r_i^2 \rangle = k_b T \sum_v \frac{e_v^2(i)}{m_i \omega_v^2} \quad (1)$$

Based on this, we calculated the crystallographic B-factors B_R for residues R of the unbound and bound states of the dimer using the technique described previously[14] via

$$B_R = \frac{8}{3}\pi^2 \frac{1}{N_R} \sum_{i \in R} \langle r_i^2 \rangle \quad (2)$$

where N_R denotes the number of atoms in residue R. The vibrational modes are related to the dynamical fluctuations of the atomic positions, and hence of the residues, around equilibrium, giving an assessment of a residue's "flexibility" or "rigidity" in each case. The B-factors of the residues in the monomeric protein subunits of the coat protein dimers before and after TR binding are shown superimposed in Fig. 2a. The B-factors of an unbound subunit are shown in black, while the red and blue lines correspond to results for the subunits that eventually transform into the A and B conformers of the TR bound dimer. We will refer to these two modified C subunits as A* and B* in the remaining analysis. Inspection of the data in Fig. 2a reveals the following: (1) The vast majority of the dynamic behavior in both bound and unbound subunits is localized in the FG-loops; (2) TR binding suppresses motion in the EF-loop that contains residues R49, S51, and S52, and connects the E and F β-strands of the B* protein subunit; and (3) TR binding enhances the flexibility of the FG-loop in subunit B*, whilst suppressing motion of this loop in subunit A*. The shifts in flexibility and rigidity of all the residues of the coat protein dimer due to the presence of RNA, that is, the B-factors for residues in an A* or B* subunit in the presence of TR minus those for these residues in a C subunit, are mapped onto the polypeptide backbone of a C/C dimer in Fig. 2b.

The all-atom normal-mode analysis shows that the four lowest-frequency vibrational modes contribute more than 90% of the total increase in flexibility of the FG-loop in the B* protein subunit, and they are localized predominantly on the FG-loops of the dimer in both the bound and unbound state. Their frequencies range from 1.79 to 3.47 cm^{-1} for the unbound dimer and from 1.87 to 3.43 cm^{-1} for the bound dimer. The modes correspond to movements of the FG-loops in correlated (i.e., the same) or anti-correlated (opposite) directions (Fig. 3a–d). The presence of the TR stem–loop does not appreciably soften any of the four lowest modes: The lowest-frequency mode increased by only 0.08 cm^{-1} from 1.79 cm^{-1}, and similar effects occur also for the other low-frequency modes. Since the frequencies of the modes are effectively unaltered, the increased flexibility of the B* subunit's FG-loop must be due to an asymmetrization of the displacement pattern resulting from TR binding, that is, equal displacements of the FG-loops for the symmetric unbound state must shift upon TR binding to favour displacements of just one FG-loop in the anti-symmetric bound state. This effect is illustrated in Fig. 3b and d where the motion of the FG-loop in the B* subunit (green) increases, while that in the A* subunit (blue) decreases, compared with the FG-loops of the unbound dimer (magenta).

In order to analyze the role of the TR stem loop in triggering this effect, its location in the bound complex needs to be taken into account. Figure 4a illustrates the contacts made by residues in an A/B dimer with TR. The backbone of TR makes contacts with residues R49, S51, and S52 in the EF-loop of the B subunit (green), while no contacts are made to this loop in the A subunit (blue). Identical contacts are of course also made in A* and B* subunits. This asymmetry in the phosphodiester contact suggests that the EF-loop in the B* subunit might be instrumental in triggering the allosteric transition from a symmetric to an asymmetric conformer. In order to test this, we performed a correlation analysis on the unbound state (symmetric dimer alone) using the correlation matrix elements

$$C_{ij} = \frac{\langle r_i r_j \rangle}{\langle r_i^2 \rangle^{1/2} \langle r_j^2 \rangle^{1/2}} \quad (3)$$

The elements were computed using the lowest 100 normal modes to assure proper convergence. The matrix elements indicate which components of the protein move in concert when averaged over many mode displacements. The analysis revealed a correlation between the EF- and FG-loops within the same protein subunit as indicated by values that ranged between 0.23 and 0.40 for correlations between residues 48–54 in the EF-loop and residues 66–82 in the FG-loop. Note that the correlation ranges to a maximum of one, denoting regions of the protein that move perfectly in concert. The computed correlations between the EF- and FG-loops are therefore significant, probably due to their connection via the F β-sheet.

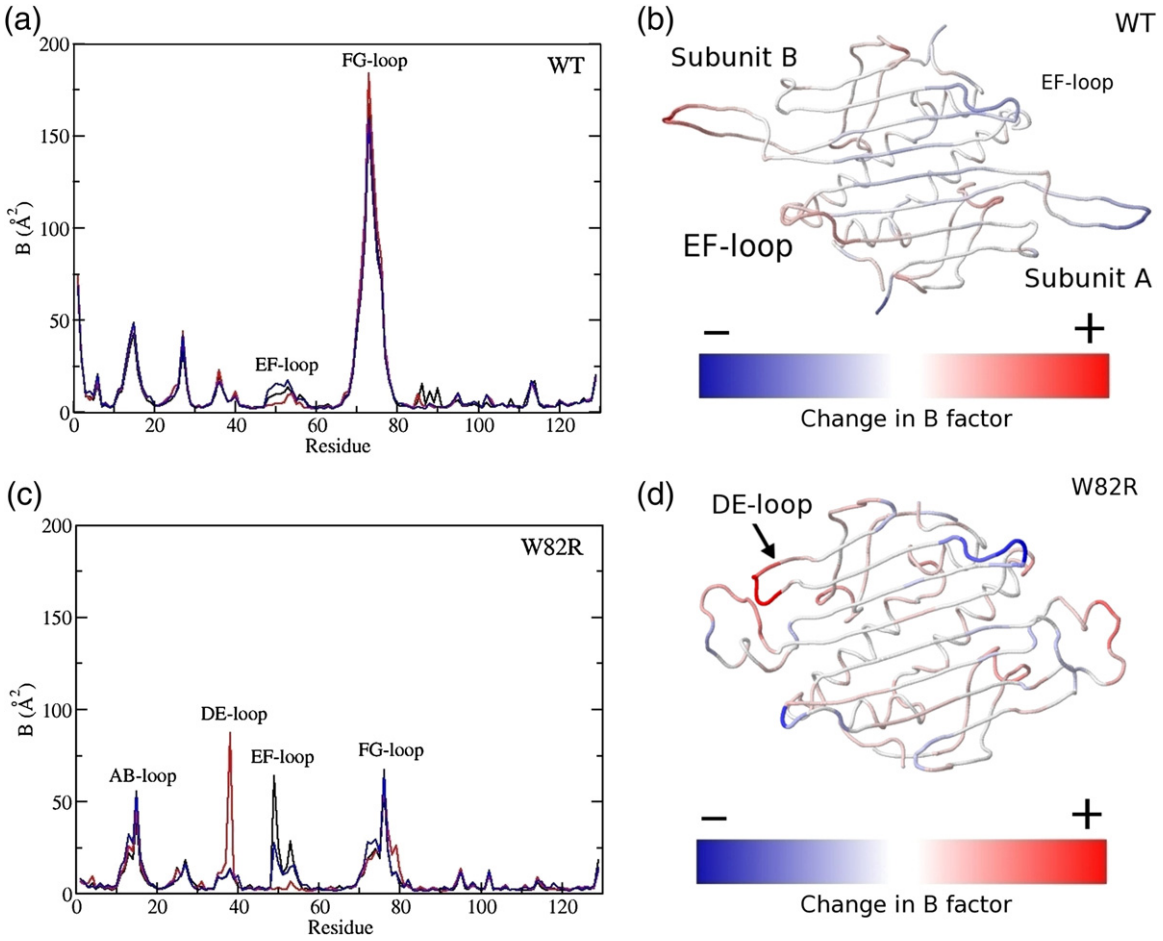

Fig. 2. Results of normal-mode analysis. (a) *B*-factors for the residues in the different protein conformers before and after TR binding. Black lines represent *B*-factors of the two minimized C/C subunits, whilst the blue and red lines indicate those of the TR-bound subunits A* and B*, respectively. The *B*-factors of atoms in the FG-loop of the B* subunit increase by 20 Å^2 (+12%), whilst those in A* decrease by 10 Å^2 (−6%). (b) The changes in *B*-factors of the residues in the wild-type dimer resulting from TR binding are shown mapped onto the polypeptide backbone of a C/C dimer, with areas of increased flexibility (+) shown in red and decreased flexibility (−) in blue. Increased flexibility is clearly discernible in the FG-loop of the B* subunit, whilst the FG-loop in the A* subunit becomes more rigid. The exposed loop in the B* subunit containing R49, S51, and S52 (EF-loop) also exhibits increased rigidity. (c) *B*-factors as in (a) for the W82R mutant. The largest shift in the *B*-factors compared with the unbound subunit occurs in the DE-loop of the B* subunit (residues 35-40) by about 40 Å^2 (+300%), and AB-loop mobility (residues 10–20) is increased by about 15 Å^2 (+37%) in the A* subunit and 7 Å^2 (+17%) in the B* subunit. EF-loop motion is inhibited in the B* subunit as expected due to its contact with the RNA stem loop. Only a small increase of 3 Å^2 (+5%) is observed for the *B*-factors of residues in the FG-loop of the B* subunit, which is significantly less than in the wild-type protein. (d) The changes in *B*-factors of the residues for the mutant dimer as in (b). The largest increase in flexibility occurs at the DE-loop, which is connected to the EF-loop via the E β-sheet. The decreased flexibility of the EF-loop due to TR binding results in enhanced mobility of the DE- rather than the FG-loop in contrast to that of the wild-type protein.

This analysis suggests the following explanation for the allosteric effect induced by TR binding to a C/C dimer: As a result of the contact between the TR phosphodiester backbone and the EF-loop of the B* subunit, the motion of this loop is suppressed. Due to its correlation with the FG-loop in the same subunit, the mobility of the FG-loop is enhanced. As this FG-loop is coupled to the FG-loop of the other protein subunit (subunit A*) in the dimer via one of the four lowest vibrational modes, the motion of the FG-loops are redistributed resulting in a repression of the flexibility of the FG-loop in the A* subunit. It is not currently possible to compute how the increased amplitudes of the lowest four frequency modes contribute to the folding of the FG-loop, and hence determine the exact pathway leading to the conformational switch. It is clear, though, that an increased amplitude of the lowest four frequency modes will result in a larger conformational space being sampled by the FG-loop. In order to estimate how strong the effect of TR binding is on the lowest-frequency vibrational mode at 1.79 cm^{-1}, we computed the average amplitude of atoms in the FG-loop (residues K66 to W82) at 300 K for both the TR-bound and RNA-free dimers using $A_i^2 = 2k_bT\eta_i^2/\omega^2$, where k_b is Boltzmann's constant, T is the temperature, ω is the frequency, and η_i^2 is the squared displacement of atom i in the mode. A comparison of the average

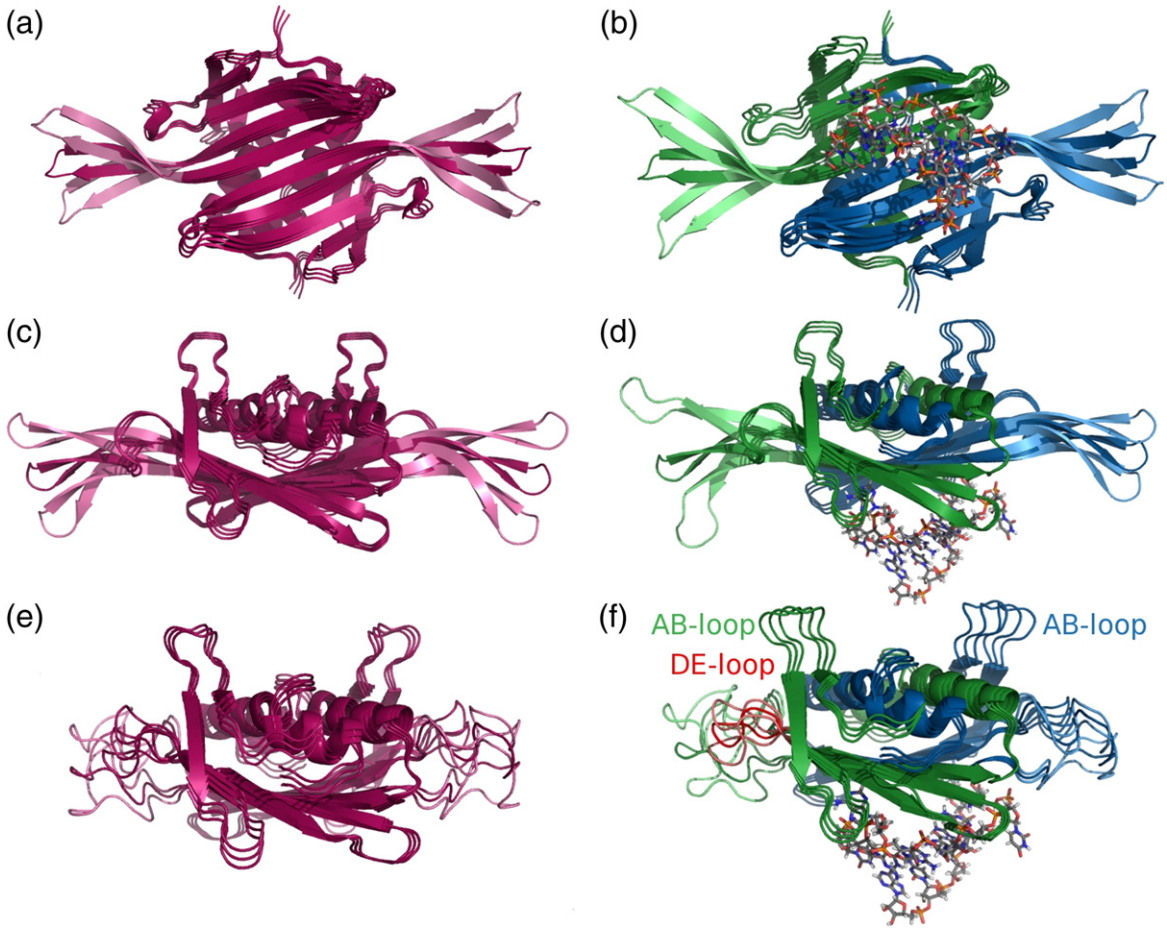

Fig. 3. Displacement patterns for the lowest-frequency modes of RNA-free and -bound states. Displacement patterns are displayed as an overlay of the minimized dimer structure and the two structures obtained by displacing that structure along the + and − directions of the normal-mode pattern. The range of motion shown is 10 times greater than the thermal amplitude ($A_i^2 = 2k_bT\eta_i^2/\omega^2$) for visual clarity. (a) and (b) are views of the dimer along the 2-fold axis from the centre of the capsid, whilst (c) and (d) are orthogonal views. (e) and (f) are views of the W82R dimer in the same orientation as the wild-type dimer pictured in (c) and (d) respectively. Low-frequency modes: (a and c) at 3.04 and 1.79 cm^{-1}, respectively, of the unbound dimer, and (b and d) at 3.04 and 1.87 cm^{-1}, respectively, of the TR-bound dimer. Motions of the FG-loop in the B* subunit increase as a result of TR binding. (e) Lowest-frequency mode at 3.68 cm^{-1} of the unbound W82R dimer, and (f) at 3.45 cm^{-1} after TR binding. The vibrational mode patterns in (e) and (f) are similar in character to those of the wild-type dimer in (c) and (d), respectively. Instead of the FG-loop becoming more dynamic as in the TR bound wild-type dimer shown in (d), the AB-loops of the A* and B* subunits and the DE-loop of the B* subunit (red) become more dynamic.

amplitudes of atoms in the FG-loop of the B* subunit of the TR bound dimer and the C subunit of the RNA-free dimer showed an increase of 41% in the average amplitude of these atoms. Similarly, a calculation of the change in the total energy (i.e., potential plus kinetic energy) of the atoms within the FG-loop revealed an increase of their total energy by 0.31 k_bT ~0.16 kcal/mol (at 300 K), which is equivalent to 31% of the total energy E_{tot} of all atoms in the mode at thermal equilibrium (i.e., of $E_{tot} = k_bT$). The impact of TR binding on the vibrational modes is therefore significant, and likely large enough to promote the rearrangements in the FG-loop (see Fig. 4b) required to form a B conformer. Further, the kinetic energy increase of 0.31 k_bT in the FG-loop of the B* protein subunit is consistent with an explanation of the allosteric effect in terms of a redistribution of protein conformational ensembles.[15] In the absence of TR, the FG-loop prefers a C-like conformational state. However, upon TR binding and contact with the EF-loop, one of the FG-loops of the dimer receives an increase in its kinetic energy (and hence also its free energy) when in the C conformation. This shifts the population of states for this FG-loop to favor the folded B conformation.

A unique feature of the FG-loop in the B conformer is the cis configuration of the peptide bond at the conserved P78, whilst it is trans in A and C subunits. This was initially suggested as the key switch specifying quasi-equivalence in this phage.[2] However, it has been shown that a mutant, P78N, forms $T = 3$ capsids as efficiently as wild-type when expressed in *E. coli*, binds TR with the same affinity as wild-type[4], and has all the peptide residues of the FG-loop of its B subunit in the trans configuration.[16] P78N, however, is not viable in an infectious clone, leading to the suggestion that it has a role in

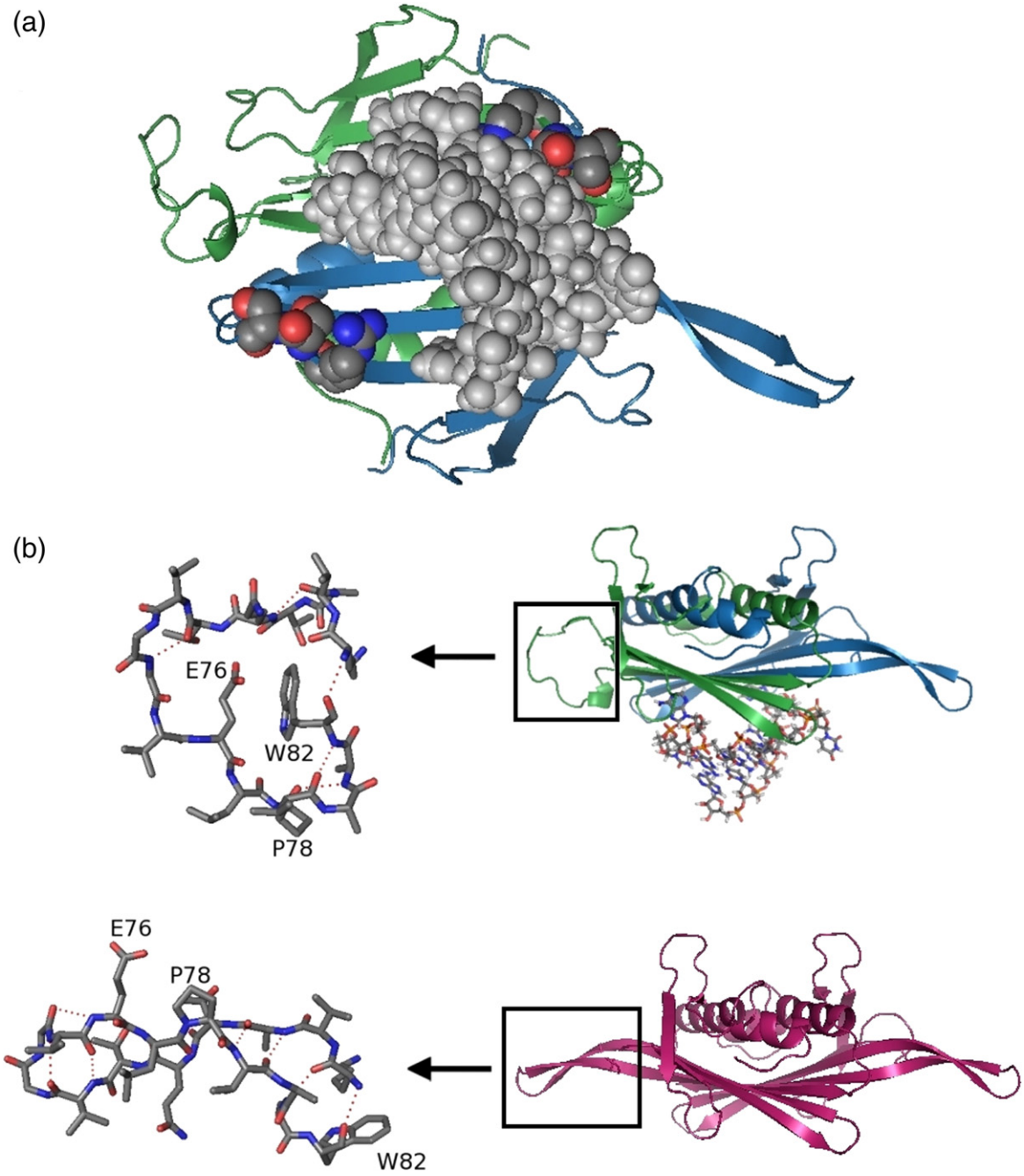

Fig. 4. A structural explanation for the allosteric effect. (a) Illustration of the contacts made by the phosphodiester backbone of the TR stem–loop with an A/B dimer (1ZDH). The EF-loops (residues 49–52) and TR are shown in space-filling representation with the RNA in gray. The phosphodiester backbone contacts the EF-loop of the B* subunit, whilst no contacts are made with the same loop in the A* subunit. (b) Close-up views of the FG-loops (residues 66–82) of B and C subunits. A comparison shows that major rearrangements take place within this loop after TR binding, for example, changes in the positions and numbers of hydrogen bonds (shown as dotted red lines), as well as the P78 isomerisation to cis in the B subunit. E76, P78, and W82 are labeled to facilitate comparison of the two conformers.

interacting with the phage maturation protein.[17] Whatever the role of P78, it is clear that the cis–trans isomerisation is not a significant factor in specifying the conformation of the FG-loop in B subunits.

As a test of the proposed allosteric mechanism, we performed a similar analysis on the assembly incompetent mutant W82R (1MSC).[18] This species binds TR normally, but does not assemble beyond the TR–dimer complex, even if chased with wild-type coat protein dimers,[5] and hence is an inhibitor of assembly. In the following analysis, we again refer to the two subunits of the mutant dimer as A* and B* relative to the position of the bound TR, even though the two subunits will not become A and B subunits after TR binding. The *B*-factors for the A* and B* subunits of the mutant in the presence of TR are shown in Fig. 2c in blue and red, respectively, while the change in *B*-factors of the dimer resulting

from TR binding are mapped onto the polypeptide backbone of a C/C dimer of the mutant in Fig. 2d. A comparison of the values with those of a subunit from an unbound dimer (see black line) shows that in contrast to the wild-type, there is no significant difference in the FG-loop mobility between the bound and unbound state (compare with Fig. 2a). Instead the *B*-factors show an enhanced flexibility of the AB-loops in both A* and B* subunits and a greater than threefold increase in flexibility of the DE-loop of the B* subunit due to TR binding. The sharp increase in the *B*-factor for the DE-loop is due to its connection to the EF-loop through the E β-strand. The W82R mutation causes an increased flexibility in the DE-loop rather than the FG-loop, in contrast to the wild-type dimer. As a result, the asymmetrization of the displacement patterns in the FG-loops of the mutant dimer after TR binding (compare Fig. 3e and f) were weaker than those observed in the wild-type (compare Fig. 3a and c with Fig. 3b and d, respectively). Additionally, the overall *B*-factors for FG-loops in the mutant dimer are approximately half of those observed in the wild-type. The FG-loops of the mutant dimer are in a unique conformation different from that of the wild-type A, B and C subunits,[17] which may account for the strongly different displacement pattern in this case of the unbound dimer when compared with the wild-type. This is likely due to the W82R mutation being within the FG-loop region and shows how the mutation results in a severe reduction in FG-loop flexibility. The results indicate that TR binding does not promote the allosteric transition from a symmetric to an asymmetric dimer in the mutant, giving a possible explanation for its inability to assemble beyond the TR complex.

Our analysis suggests that the allosteric effect depends only on the contact of the TR phosphodiester backbone with the EF-loop in the B* subunit. It is thus non-sequence-specific and can equally be triggered by other stem–loops, for example those discussed in Basnak *et al.*[6] Although the stem–loops used in those experiments have variations when compared with TR such as their length or coat protein affinity, it is known that all the stem–loops bind to MS2 coat protein dimer in the same way as TR.[19–21] Thus, these differences do not alter the fundamental contact made with the EF-loop; hence, the analysis predicts that the allosteric effect would be preserved in these stem–loops. This has important implications for the assembly process of the particle: It suggests that via other non-TR stem–loops, the genome can exert a cooperative effect on the formation of the protein container beyond the initiation step by facilitating the switching of symmetric into asymmetric dimers at any of the 60 locations of the A/B dimers in the capsid. This sheds new light on the processes underlying RNA virus assembly and the roles of the RNA in facilitating the assembly process. For example, the possibility of stem–loops other than TR triggering the allosteric switch from C/C to A/B dimer is a prerequisite for the recently proposed Hamiltonian paths model in Toropova *et al.*[22] That model shows how the vast complexity of all possible combinatorial assembly pathways is drastically reduced when assembly follows the Hamiltonian paths defined by the polyhedron of genomic RNA underneath the protein shell seen in the cryo-electron microscopy reconstruction.[22] This in principle makes the modeling of assembly pathways tractable.

Acknowledgements

This work was supported by grants from The Leverhulme Trust (R.T.) and the BBSRC (P.G.S.). R.T. also thanks the Trust for a Research Leadership Award. We thank our colleagues in York and Leeds for many helpful discussions of this manuscript.

References

1. Valegard, K, Liljas, L., Fridborg, K. & Unge, T. (1990). The three-dimensional structure of the bacterial virus MS2. *Nature*, **345**, 36–41.
2. Golmohammadi, R., Valegard, K., Fridborg, K. & Liljas, L. (1993). The refined structure of bacteriophage MS2 at 2.8 Å resolution. *J. Mol. Biol.* **234**, 620–639.
3. Stockley, P. G., Stonehouse, N. J. & Valegard, K. (1994). Molecular mechanism of RNA phage morphogenesis. *Int. J. Biochem.* **26**, 1249–1260.
4. Lago, H., Parrott, A. M., Moss, T., Stonehouse, N. J. & Stockley, P. G. (2001). Probing the kinetics of formation of the bacteriophage MS2 translational operator complex: identification of a protein conformer unable to bind RNA. *J. Mol. Biol.* **305**, 1131–1144.
5. Stockley, P. G., Rolfsson, O., Thompson, G. S., Basnak, G., Francese, S., Stonehouse, N. J. *et al.* (2007). A simple, RNA-mediated allosteric switch controls the pathway to formation of a $T=3$ viral capsid. *J. Mol. Biol.* **369**, 541–552.
6. Basnak, G., Morton, V. L., Rolfsson, O., Stonehouse, N. J., Ashcroft, A. E. & Stockley, P. G. (2009). Viral genomic ssRNA directs the pathway towards a $T=3$ capsid. *J. Mol. Biol.* **395**, 924–936.
7. Peabody, D. S. & Ely, K. R. (1992). Control of translational repression by protein-protein interactions. *Nucleic Acids Res.* **20**, 1649–1655.
8. Tama, F. & Brooks, C. L., III (2005). Diversity and identity of mechanical properties of icosahedral viral capsids with elastic network normal mode analysis. *J. Mol. Biol.* **345**, 299–314.
9. Dykeman, E. C. & Sankey, O. F. (2008). Low frequency mechanical modes of viral capsids: an atomistic approach.*Phys. Rev. Lett.* **100**, 028101.
10. Cornell, W. C., Cieplak, P., Bayly, C. I., Gould, I. R. Merz Jr., K. M., Ferguson, D. M. *et al.* (1995). A second generation force field for the simulation of proteins, nucleic acids, and organic molecules. *J. Am. Chem. Soc.* **117**, 5179–5197.
11. Tsui, V. & Case, D. A. (2001). Theory and applications of the generalized Born solvation model in macromolecular simulations. *Biopolymers*, **56**, 275–291.
12. Valegard, K., Murray, J. B., Stonehouse, N. J., van den Worm, S., Stockley, P. G. & Liljas, L. (1997).

The three-dimensional structures of two complexes between recombinant MS2 capsids and RNA operator fragments revel sequence-specific protein-RNA interactions. *J. Mol. Biol.* **270**, 724–738.
13. van Vlijmen, H. W. T. & Karplus, M. (2005). Normal mode calculations of icosahedral viruses with full dihedral flexibility by use of molecular symmetry. *J. Mol. Biol.* **350**, 528–542.
14. Kuriyan, J. & Weis, W. (1991). Rigid protein motion as a model for crystallographic temperature factors. *Proc. Natl. Acad. Sci. USA*, **88**, 2773–2777.
15. Gunasekaran, K., Ma, B. & Nussinov, R. (2004). Is allostery an intrinsic property of all dynamic proteins? *Proteins: Struct. Funct. Bioinf.* **57**, 433–443.
16. Stonehouse, N. J., Valegard, K., Golmohammadi, R., van den Worm, S., Walton, C., Stockley, P. G. & Lilljas, L. (1996). Crystal structures of MS2 capsids with mutations in the subunit FG loop. *J. Mol. Biol.* **256**, 330–339.
17. Hill, H. R., Stonehouse, N. J., Fonseca, S. A. & Stockley, P. G. (1997). Analysis of phage MS2 coat protein mutants expressed from a reconstituted phagemid reveals that proline 78 is essential for viral infectivity. *J. Mol. Biol.* **266**, 1–7.
18. Ni, C.-Z., Syed, R., Kodandapani, R., Wickersham, J., Peabody, D. S. & Ely, K. R. (1995). Crystal structure of the MS2 coat protein dimer: implications for RNA binding and virus assembly. *Structure*, **3**, 255–263.
19. Horn, W. T., Tars, K., Grahn, E., Helgstrand, C., Baron, A. J. & Lago, H. (2006). Structural basis of RNA binding discrimination between bacteriophage Qbeta and MS2. *Structure*, **14**, 487–495.
20. Convery, M. A., Rowsell, S., Stonehouse, N. J., Ellington, A. D., Hirao, I., Murray, J. B. *et al.* (1998). Crystal structure of an RNA aptamer-protein complex at 2.8 Å resolution. *Nat. Struct. Biol.* **5**, 133–139.
21. Rowsell, S., Stonehouse, N. J., Convery, M. A., Adams, C. J., Ellington, A. D., Hirao, I. *et al.* (1998). Crystal structures of a series of RNA aptamers complexed to the same protein target. *Nat. Struct. Biol.* **5**, 970–975.
22. Toropova, K., Basnak, G., Twarock, R., Stockley, P. G. & Ranson, N. A. (2008). The three-dimensional structure of genomic RNA bacteriophage MS2: Implications for assembly. *J. Mol. Biol.* **375**, 824–836.